Membrane Restructuring by Phospholipase A_2 Is Regulated by the Presence of Lipid Domains

Chad Leidy,[†*] Jackson Ocampo,[†] Lars Duelund,[‡] Ole G. Mouritsen,[‡] Kent Jørgensen,[§] and Günther H. Peters[§]
[†]Department of Physics, Universidad de los Andes, Bogotá, Colombia; [‡]MEMPHYS-Center for Biomembrane Physics, Department of Physics and Chemistry, University of Southern Denmark, Odense, Denmark; and [§]MEMPHYS-Center for Biomembrane Physics, Department of Chemistry, Technical University of Denmark, Lyngby, Denmark

ABSTRACT Secretory phospholipase A_2 ($sPLA_2$) catalyzes the hydrolysis of glycerophospholipids. This enzyme is sensitive to membrane structure, and its activity has been shown to increase in the presence of liquid-crystalline/gel (L_α/L_β) lipid domains. In this work, we explore whether lipid domains can also direct the activity of the enzyme by inducing hydrolysis of certain lipid components due to preferential activity of the enzyme toward lipid domains susceptible to $sPLA_2$. Specifically, we show that the presence of L_α/L_β and $L_\alpha/P_{\beta'}$ phase coexistence in a 1,2-dimyristoyl-*sn*-glycero-3-phosphocholine (DMPC)/1,2 distearoyl-*sn*-glycero-3-phosphocholine (DSPC) system results in the preferential hydrolysis of the shorter-chained lipid component in the mixture, leading to an enrichment in the longer-chained component. The restructuring process is monitored by atomic force microscopy on supported single and double bilayers formed by vesicle fusion. We observe that during preferential hydrolysis of the DMPC-rich L_α regions, the L_β and $P_{\beta'}$ regions grow and reseal, maintaining membrane integrity. This result indicates that a sharp reorganization of the membrane structure can occur during $sPLA_2$ hydrolysis without necessarily destroying the membrane. We confirm by high-performance liquid chromatography the preferential hydrolysis of DMPC within the phase coexistence region of the DMPC/DSPC phase diagram, showing that this preferential hydrolysis is accentuated close to the solidus phase boundary. Differential scanning calorimetry results show that this preferential hydrolysis in the presence of lipid domains leads to a membrane system with a higher-temperature melting profile due to enrichment in DSPC. Together, these results show that the presence of lipid domains can induce specificity in the hydrolytic activity of the enzyme, resulting in marked differences in the physical properties of the membrane end-product.

INTRODUCTION

Secretory phospholipase A_2 ($sPLA_2$) enzymes catalyze the hydrolysis of the ester linkage in the $sn-2$ position of glycerophospholipids, yielding free fatty acids (FFA) and lysophospholipids (1). These low-molecular-weight enzymes are functionally diverse, playing a broad range of physiological roles that result from their ability to either generate signaling molecules (1) or degrade cell membranes (2,3). Many of the human isoforms of $sPLA_2$ have been associated with the inflammation process. This has been inferred from the overexpression of these enzymes during the inflammatory response and due to the production of arachidonic acid and lysophospholipids, which serve as precursors to a variety of proinflammatory molecules (4). The ability of secretory $sPLA_2$ to degrade membranes plays an important role during the inflammatory response. One of the human isoforms, $sPLA_2$-IIA has been associated with the hydrolysis of Gram-positive bacterial membranes (5), therefore acting as an antibacterial agent in certain bacterial infections. Dead or damaged cells also become susceptible to $sPLA_2$-IIA. It has been suggested that this activity serves as a clearance mechanism during cellular waste management (2).

Several membrane physical properties, such as the membrane curvature and pressure profile (6–8), membrane mechanical stretching and bending constants (9), and membrane lateral organization (10–12), are controlled by lipid composition. In this scenario, the hydrolytic activity of $sPLA_2$ has the potential to regulate cell-membrane physical properties by modifying cell-membrane composition. For example, $sPLA_2$ has been shown to stimulate exocytosis and neurotransmitter release in pheochromocytoma-12 cells and hippocampal neurons (13), most likely by promoting membrane fusion and fission through regulation of membrane curvature. $sPLA_2$has also been studied in relation to neuronal lipid membrane repair and regeneration (3). In this case, it was shown that $sPLA_2$ is necessary for membrane sealing after damage and for the formation of a new growth cone. For these processes to take place without loss of membrane integrity, $sPLA_2$ activity must be carefully regulated. However, it is not yet clear whether $sPLA_2$ activity can be directed in a manner that leads to a desired compositional end-product while avoiding indiscriminate hydrolysis of other lipid components. In this work, we explore whether the physical properties of the membrane can lead to a directed hydrolytic process. In particular, we are interested in exploring whether the presence of lipid domains can induce specificity in the activity of the enzyme, leading to a desired end-product.

Through the modulation of lipid packing, lipid domains have been shown to influence $sPLA_2$ activity. For example, coexistence of lipid domains generates packing defects at

Submitted May 4, 2010, and accepted for publication February 24, 2011.

*Correspondence: cleidy@uniandes.edu.co

Editor: Thomas J. McIntosh.

0006-3495/11/07/0090/10 $2.00

doi: 10.1016/j.bpj.2011.02.062

the domain interface, which, by weakening lipid interactions, can enhance the hydrolytic rate (14–17). With regard to native cell membranes, heterogeneities that arise in erythrocyte membranes as a result of ionophore-induced calcium intake have been shown to increase susceptibility to $sPLA_2$ (18).However, in addition to regulating susceptibility, can domains also regulate specificity? Recently, it was shown (19) that $sPLA_2$ activity on ternary DOPC/DPPC/Chol membranes presenting liquid-ordered/liquid-disordered phase coexistence, leads to a shrinkage in the liquid-disordered regions, suggesting preferential hydrolysis of the lipid components enriched in the liquid-disordered regions.

In this work, we are interested in exploring by atomic force microscopy (AFM) the ability of $sPLA_2$ to induce membrane restructuring through preferential hydrolysis of membrane components in the presence of lipid domains. Supported single and double 1,2-dimyristoyl-*sn*-glycero-3-phosphocholine (DMPC)/1,2 distearoyl-*sn*-glycero-3-phosphocholine (DSPC) bilayers are formed through vesicle fusion. This technique has proven to maintain macroscopic membrane dynamics even when the membrane is in close proximity to the support, allowing the exploration of membrane restructuring phenomena (20–22). In addition, based on the AFM results, we explore in vesicle suspensions how the presence of lipid domains can direct the preferential hydrolysis of one of the lipid components. This preferential hydrolysis leads to a significant shift in the melting profile of the end-products of the hydrolytic reaction.

MATERIALS AND METHODS

DMPC, and DSPC were purchased from Avanti Polar Lipids (Alabaster, AL) and were used without further purification. Snake venom $sPLA_2$ (*Agkistrodon piscivorus piscivorus*) was a gift from Prof. R. L. Biltonen, University of Virginia (Charlottesville, VA). Ruby Muscovite mica was obtained from Plano W. Plannet (Wetzlar, Germany).

Formation of supported lipid bilayers

Appropriate amounts of DMPC and DSPC were dissolved and mixed in chloroform. The samples were then dried under nitrogen gas and placed under vacuum overnight to remove the residual solvent. The dried lipids were dispersed in Milli-Q water (Millipore, Billerica, MA) to a final concentration of 3 mM. Aqueous multilamellar lipid dispersions were prepared by heating the samples to 65°C and then vortexing. Small unilamellar vesicles (SUVs) were prepared by sonication using a Labsonic U tip sonicator (B. Braun Biotech International, Melsungen, Germany) at 65°C for two 7-min periods. Residual titanium arising from the tip was removed from the vesicle solution by centrifugation for 5 min at 2750 × *g*. The SUVs were immediately rewarmed to 65°C, and 1 ml was added to a small home-built cell for the AFM containing a piece of freshly cleaved mica. The samples were incubated for 1 h, at 24°C. The samples were then rinsed by exchanging the incubation solution 10 times with 20 mM NaCl solution and 20 μM $CaCl_2$ (required for $sPLA_2$ activity), never allowing the supported bilayer to dry. Adding the warmed SUV solution and allowing the sample to cool down during incubation to a temperature below the solidus phase was generally a successful procedure for obtaining double bilayers. Single bilayers were usually obtained when the SUVs were cooled to room temperature before adding the solution onto the freshly cleaved mica.

Atomic force microscopy

The mica-supported lipid bilayers were imaged in contact mode using a PicoSPM AFM (Molecular Imaging, Phoenix, AZ). The cantilevers were oxide-sharpened silicon nitride cantilevers (ThermoMicroscopes, Sunnyvale, CA) with nominal spring constants of 0.01 N/m (Figs. 1–4) and 0.02 N/m. To ensure that the force was kept minimal during scanning, the force was frequently decreased until the tip left the surface and subsequently slightly increased until it just regained contact. Due to scanner hysteresis and small variations in temperature during scanning, precise statements about the scanning force are difficult to make. Even temperature fluctuations of the order of 10^{-2}°C cause noticeable thermal bending of the gold-coated cantilevers. However, a conservative estimate of the force range would be 20–300 pN based on the nominal spring constant. $sPLA_2$ was added to give a total concentration of ~420 nM. The total lipid concentration of the solid-supported lipid bilayer system in the AFM fluid cell was ~2 μM. The protein/lipid ratio is then 1:5. All image analyses were performed using SPIP (Image Metrology, Hørsholm, Denmark).

Differential scanning calorimetry for determination of the DMPC/DSPC phase diagram

Appropriate amounts of DMPC and DSPC were dissolved and mixed in chloroform. The samples were then dried under nitrogen gas and placed under vacuum overnight to remove the residual solvent. The dried lipids were dispersed in Milli-Q water to a final concentration of 50 mM. Aqueous multilamellar lipid dispersions were prepared by heating the samples to 65°C and then vortexing. This procedure was repeated for 15 min. DSC was performed using a MicroCal MC-2 (Northhampton, MA) on samples at a scan rate of 10°C/h. A DSC scan was also performed on the buffer solution and was

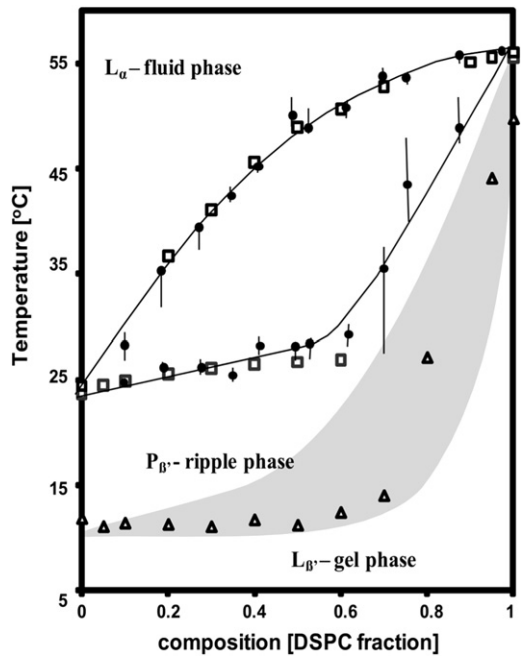

FIGURE 1 DMPC/DSPC phase diagram constructed from DSC data. The fluidus and solidus phase lines were determined from the onset and completion of the melting event in the thermograms (*open squares*). We have superimposed (*solid circles*) data from Mabrey and Sturtevant (24). We have also added the pretransition line (*open triangles*) to emphasize that the ld/so coexistence regime presents coexistence of the ripple phase and L_α phase (20). The gray area represents an estimated region of $P_{\beta'}/L_\beta$ coexistence.

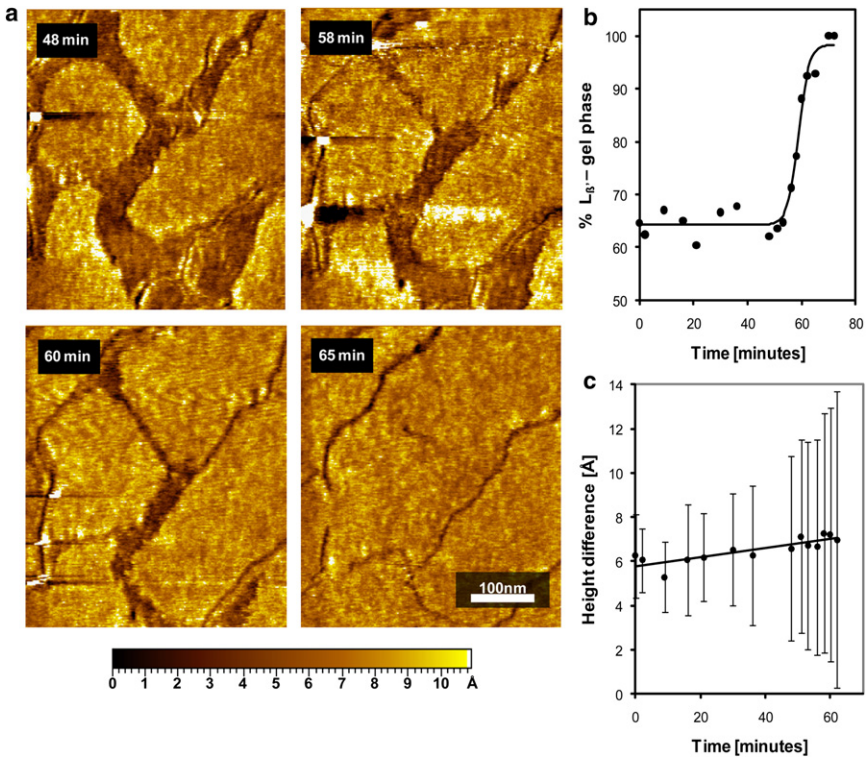

FIGURE 2 (*a*) AFM imaging of $sPLA_2$-induced L_α-phase domain shrinking accompanied by L_β-phase domain merging in a single supported bilayer of a 1:1 DMPC/DSPC mixture visualized at 30°C. The L_α-phase domains appear darker due to the reduced height, as indicated by the height scale. (*b*) The L_β-phase area fraction as a function of time after addition of $sPLA_2$. The system exhibits a lag phase before the hydrolytic burst, which occurs ~58 min after addition of $sPLA_2$. (*c*) We do not observe a change in the relative height difference between the L_β and the L_α phase during the hydrolytic burst; however, heterogeneities do emerge, as is apparent from the increase in the error bars.

used to subtract a baseline from the thermograms of the different DMPC/DSPC mixtures. The onset and completion temperatures used to compose the DMPC/DSPC phase diagram were determined by the intersection of the slope line at half-width of the peak heat capacity with the baseline. We identify the pretransition temperature by determining the peak position.

Fluorescence spectroscopy and differential scanning calorimetry of $sPLA_2$-treated samples

Samples studied by DSC after treatment with $sPLA_2$ (see Fig. 6) were prepared as follows. $sPLA_2$hydrolysis was monitored by following the release of a water-soluble fluorescent dye, calcein, encapsulated in DMPC/DSPC LUVs (200 nm) in a self-quenching concentration (50 mM) as described previously (22). The intact vesicles containing calcein present a low level of fluorescence due to self-quenching. As $sPLA_2$ acts on the vesicles, and calcein is released into the medium, an increase in fluorescence intensity is registered due to the dilution of calcein. We briefly describe the sample preparation. Calcein was dissolved in water and pH was adjusted to 7.5 with NaOH before adding the calcein solution to the 10 mM HEPES buffer (10 mM HEPES, 1 mM KCl, 1 mM NaN_3, 30 μM $CaCl_2$, and 10 μM NaEDTA). The lipid suspension was hydrated in the calcein solution as described above. The multilamellar vesicles were extruded 10 times through two stacked polycarbonate filters with 200-nm pore size (Whatman, Clifton, NJ), forming large unilamellar vesicles (LUVs) with a narrow size distribution. Untrapped calcein was removed from the liposome suspension by gel filtration through a column packed with Sephadex G-50 using the HEPES buffer as eluent. The final lipid concentration was adjusted to 1.2 mM using the HEPES buffer. Fluorescence measurements were performed using an SLM DMX 1100 spectrofluorometer (SLM Instruments, Urbana, IL). Excitation and emission channels were set at 490 nm and 515 nm, respectively, and fluorescence was measured as a function of time. $sPLA_2$ was added after 100 s, and fluorescence was monitored to detect the enzyme burst behavior, which appeared as a clearly defined burst in fluorescence. The hydrolytic reaction was quenched 600 s after the hydrolytic burst by adding 40 μl of 10 mM EDTA, and 1.5 ml of the hydrolyzed sample was placed in the DSC sample cell, with HEPES buffer in the reference cell. DSC was performed using a MicroCal MC-2 on samples at a scan rate of 10°C/h. A DSC scan was also performed on the buffer solution and was used to subtract a baseline from the thermograms of the different $sPLA_2$-treated DMPC/DSPC samples.

The sloped baselines observed in the thermograms reported in Fig. 6 are explained by the low concentration of lipids necessary to perform these scans (1.2 mM). These low concentrations result in very subtle thermal events. By zooming in with the purpose of distinguishing the melting events, small differences in the sample and reference baselines become evident during subtraction (leading to the sloping baselines). The low concentration of lipids is necessary because a compromise had to be reached between obtaining an observable melting event by DSC and using a lipid concentration low enough to ensure a homogeneous $sPLA_2$ hydrolysis process. Our intention with these DSC scans is to show qualitatively the shifts in the melting profile induced by the hydrolytic activity of the enzyme, not to quantify the melting event, since this would not yield precise information due to the low concentrations used.

High-performance liquid chromatography

Quantification of the hydrolysis reaction by high-performance liquid chromatography (23) was made using a Waters 2010 system (Milford, MA) equipped with a Waters 510 pump, a Waters 717 Plus autosampler, and a PL-EMD 950 evaporative light-scattering mass detector from Polymer Laboratories (Cheshire, UK) using a 5-mm Phenomenex (Torrance, CA) diol spherical column and a mixture of chloroform/methanol/water (73:23:3 v/v) as the isocratic mobile phase. Lipid suspension samples of 100 μl were retrieved directly from the reaction chamber in the fluorometer during the $sPLA_2$ lipid hydrolysis time course 600 s after the hydrolytic burst using the same protocol as described in the previous section. The extracted lipids were rapidly mixed in chloroform/methanol/acetic acid/water (2:4:1:1) to quench the $sPLA_2$ lipid hydrolysis effectively. Tests were carried out to confirm that the composition of the sample did not

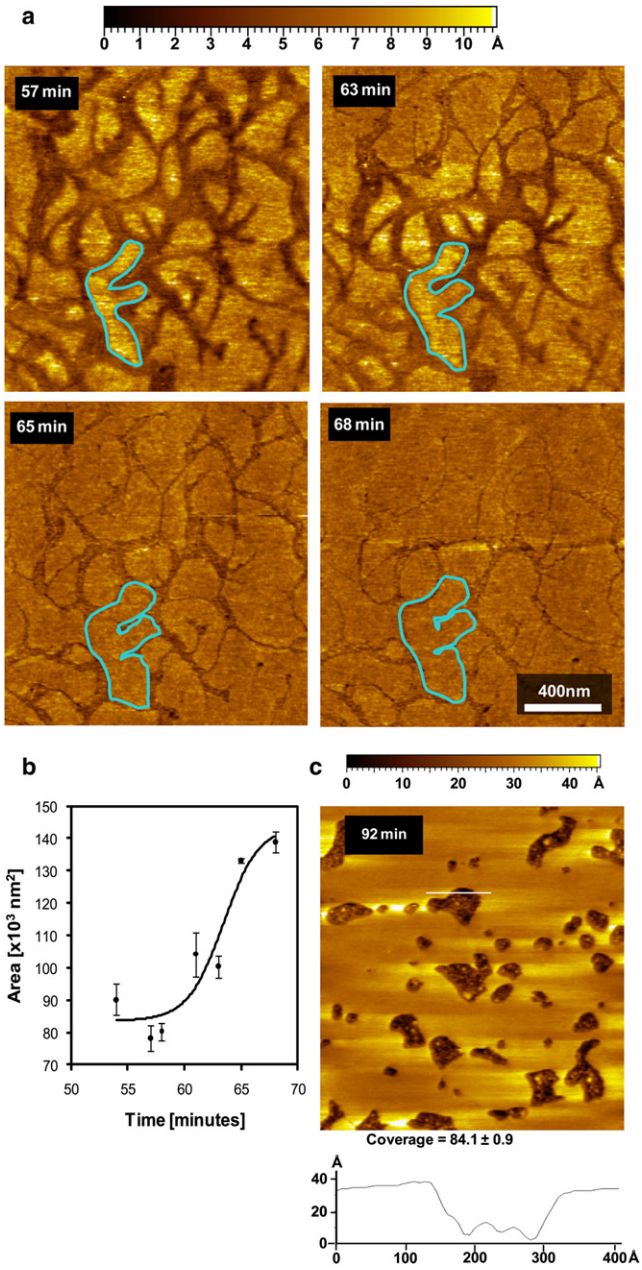

FIGURE 3 (*a*) Monitoring the area of a single L_β-phase domain in a single supported bilayer of a 1:1 DMPC/DSPC mixture visualized at 30°C during sPLA$_2$ hydrolysis. (*b*) Burst behavior of the hydrolytic event occurring ~60 min after addition of sPLA$_2$, as monitored by measuring the area increase of the L_β-phase domain. (*c*) Zoom-out after the hydrolytic burst to show the formation of holes in the supported bilayer due to loss of membrane components during the hydrolytic burst. Monitoring for 30 min after the hydrolytic burst shows that this structure is stable in the continued presence of sPLA$_2$. The 40-Å height difference shown in the height profile (*white line on image and lower graph*) demonstrates that the dark areas represent holes in the membrane.

change by storage after quenching the sPLA$_2$ activity. Salts were extracted from the sample by shaking thoroughly with 1 ml water. From the organic phase, 20 μl was analyzed by high-performance liquid chromatography. The degree of hydrolysis was measured by the reduction in the substrate fraction. Dose calibration curves were linear in the concentration range used.

RESULTS AND DISCUSSION

Mapping the DMPC/DSPC phase diagram

The DMPC/DSPC binary system is used as a model system to explore the activity of sPLA$_2$ in the presence of lipid domains. The phase behavior of this binary mixture has been studied extensively, providing a clearly defined system with well-established phase boundaries (10,20,24). Fig. 1 shows a phase diagram for the DMPC/DSPC binary system constructed from DSC thermograms for different lipid ratios (Fig. 1, *open squares*). We have superposed the phase diagram developed by Mabery and Stutevant (24) showing the fluidus- and solidus-phase lines enclosing the coexistence regime. The two data sets agree very closely.

We have also added data for the pretransition temperature, which indicate the formation of the ripple phase (Fig. 1, *open triangles*). Although the pretransition generally varies depending on the history of the sample, being particularly sensitive to cooling scans (25), we find that storing the samples overnight at 4°C and scanning in the heating direction at 2°C/h generate reproducible results. Storing at 4°C allows the system to relax completely into the gel phase, thereby ensuring that the system is in thermodynamic equilibrium before the heating scan.

Not much work has been reported on mapping carefully the position of the pretransition in this binary phase diagram—in particular due to the difficulty in ensuring that the pretransition temperature is measured under thermodynamic equilibrium conditions. However, we are interested in mapping out in detail the ripple-phase region in the DMPC/DSPC for two reasons. First, previous work in our lab has shown that the ripple phase persists above the solidus phase line (20–22), and therefore playing an important role in the structural properties of lipid domains for this system. Second, sPLA$_2$ activity appears to be very sensitive to the presence of the ripple phase, and therefore, knowing what composition and temperature regions are associated with the ripple phase is relevant for our study (22). Our data show that the pretransition merges with the main melting event between 80 and 95 mol % DSPC (Fig. 1), most likely indicating that the ripple phase vanishes in this composition regime. Additional phase diagrams have been proposed for this system. In particular, Knoll and Sackmann studied through small-angle neutron scattering on sonicated DMPC/DSPC liposomes the region below the solidus phase line (26). Their results suggest the presence of solid-solid phase coexistence below the solidus phase line. However, those authors do not present evidence regarding ripple-phase formation because they used sonicated vesicles, which have a high degree of curvature that inhibits ripple-phase formation. Previous AFM data from our group show that the DMPC/DSPC system presents full coverage of ripples below the solidus phase line and above the pretransition, suggesting the presence of only one phase below the solidus phase line, at least for the 1:1 DMPC/DSPC

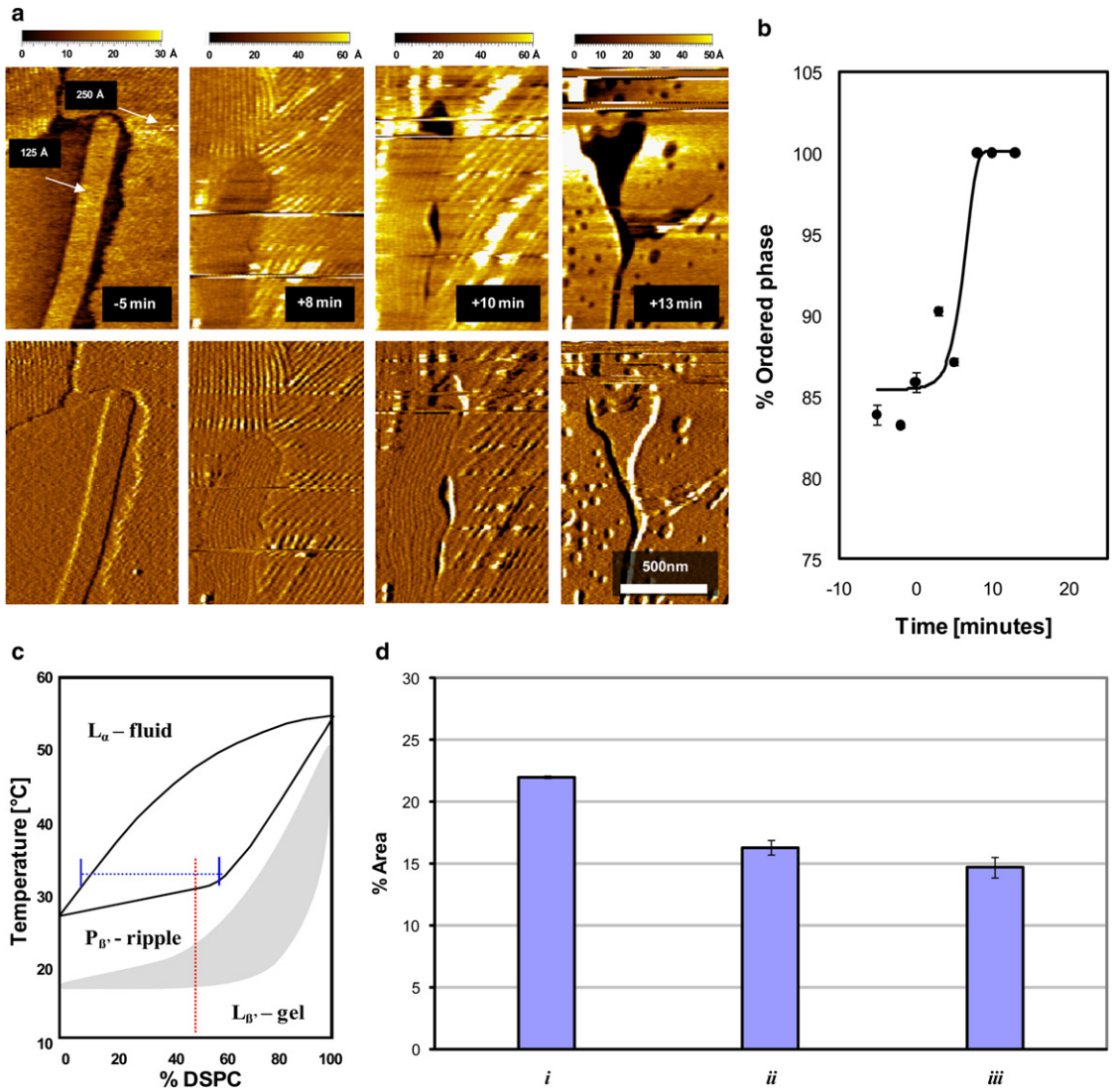

FIGURE 4 (*a*) Height difference and phase-contrast imaging of $sPLA_2$-induced membrane restructuring of the second bilayer in a supported double bilayer of a 1:1 DMPC/DSPC mixture visualized at 30°C. Before hydrolysis (−5 min), the membrane exhibits ripple ($P_{\beta'}$) domains, in coexistence with L_α-phase domains (20). As hydrolysis proceeds, a shrinkage in the fluid-phase regions and a broadening and collapse in the ripple structure is simultaneously observed, resulting in a flat L_β-phase membrane. Holes are seen to emerge after the hydrolytic burst. (*b*) The L_β-phase area fraction as a function of time after addition of $sPLA_2$. (*c*) Phase diagram and tie line indicating the fraction of L_β and L_α phase expected for the conditions in *a*. (*d*) Comparison between 1), the fraction of fluid-phase domains predicted by the tie line in *c*, 2), the area fraction of fluid-phase area measured by AFM, and 3), the area fraction of holes present in the image after the hydrolytic burst.

composition (20–22). However, it is important to note that the position of the pretransition peak moves sharply upward in temperature with increasing DSPC. This necessarily indicates the presence of a $P_{\beta'}/L_\alpha$ coexistence region. We indicate in Fig. 1 a region of uncertainty (*gray area*) where this coexistence regime may lie. However, further work is necessary to solve this discrepancy. For this work, it is sufficient to know that the DMPC/DSPC system presents a ripple-phase region below the solidus phase line of the systems to be studied. Therefore, DMPC/DSPC mixtures between the solidus phase line and the fluidus phase line will present $P_{\beta'}/L_\alpha$ coexistence.

Dynamic healing of L_β regions during preferential hydrolysis of L_α domains by $sPLA_2$

Fig. 2 shows height-mode AFM images of a 1:1 DMPC/DSPC supported single bilayer at 30°C formed by vesicle fusion in the presence of $sPLA_2$. The images show coexisting L_β and L_α domains, which appear as lighter and darker areas, respectively. The average height difference between the L_α- and L_β-phase regions was measured to be 6 ± 2 Å, which is smaller than previously reported height differences between fluid-phase and gel-phase domains for the DLPC/DSPC and DMPC/DSPC systems (27,28). We explain this reduced height difference by the fact that at

30°C, we are close to the solidus phase line, and the ordered phase domains are enriched in the shorter DMPC. The domain boundaries are, however, well defined. The L_β domains are flat and do not show evidence of ripple formation. This contradicts the phase diagram in Fig. 1, which indicates that ripples (L_β phase) should be present in coexistence with the L_α at this temperature (22). The flattened ordered domains are caused by the influence of the mica support on the supported single bilayer. We have previously shown that ripple formation is hindered in the proximal bilayer due to interactions with the surface. Ripples only form in multiple bilayer stacks spatially removed from the support. The absence of ripple formation allows us to use the supported single bilayer in Fig. 2 *a* as a model for L_α/L_β phase coexistence during $sPLA_2$ hydrolysis. Later (Fig. 4), we turn our attention to supported double bilayers, which do present ripple $P_{\beta'}/L_\alpha$ phase coexistence.

Four sequential images (Fig. 2 *a*) are taken at different times after $sPLA_2$ addition, as noted at the upper left of each image. At 48 min, the domain structure observed is identical to the original domain structure before $sPLA_2$ addition. At this point in time, the sample is still within the lag period of enzyme activity, therefore showing very low hydrolysis levels (29). The length of the lag period is influenced by the interaction of the membrane with the surface. This can be seen when comparing with the lag period observed in a double bilayer system (Fig. 4), where the hydrolyzed membrane is separated from the surface by a spacer membrane. At ~58 min, a burst in enzymatic activity is observed, characterized by a steady increase in the L_β-phase regions. In Fig. 2 *b*, the area percentage covered by the L_β phase is plotted as a function of time after addition of $sPLA_2$. The plot clearly shows a lag period where the percentage of L_β phase remains steady at ~65% followed by a burst period where the percentage of L_β phase reaches 100%. The lag-burst behavior is a trademark of $sPLA_2$ activity on saturated PC bilayers (29,30). The burst is believed to occur due to an increase in the local level of defects induced by a slow product accumulation during the lag period (29). These defects catalyze the activity of the enzyme and induce the burst behavior. This preferential hydrolysis has been reported previously for L_α/L_β domain coexistence in giant unilamellar vesicles (31) and by AFM on Langmuir-Blodget (LB) films (32). The images also show that the gel-phase domains grow and cover the space left by the hydrolyzed fluid phase.

The dynamic healing observed in Fig. 2 indicates that the supported bilayer presents a high level of mobility which allows lipid rearrangement. This mimics the behavior of free-standing bilayers observed by Sanchez et al. (31). That group reported preferential hydrolysis and gradual shrinkage of the fluid phase during $sPLA_2$ activity on giant unilamellar vesicles presenting L_α/L_β domain formation. However, our results contradict previous studies on supported bilayers treated with $sPLA_2$. The common observation in these studies is the emergence of small holes that grow steadily in time during $sPLA_2$ activity (29,32). The membranes lack the capability to rearrange and heal during hydrolysis. The explanation of this difference in membrane behavior lies in the preparation method. Previous studies on $sPLA_2$ hydrolysis of supported bilayers have in common that the supported bilayers are formed by LB deposition instead of vesicle fusion. It is apparent from these results that the supported bilayers formed by LB deposition do not show a high degree of dynamic behavior. This could be explained by the dehydration induced during the upward deposition of the first monolayer.

In Fig. 2 *c*, we attempt to detect changes in the coexistence interface height difference during the hydrolytic burst. We do not observe any significant change in the height difference between the L_β and the L_α domains. We do, however, detect an increase in the standard deviation of the height differences within the burst period. This indicates the appearance of heterogeneities in the domain interface, which could be a result of enzyme binding and/or accumulation of hydrolysis products. This would lead to a more heterogeneous interface and the formation of protrusions due to the presence of additional lipid species and the bound enzyme, which is ~5 nm in size.

Growth of L_β domains during preferential hydrolysis of L_α domains by $sPLA_2$

In Fig. 3, we monitor a single L_β-phase domain (*outlined area*) as a function of time during $sPLA_2$ hydrolysis. In Fig. 3 *b*, the domain area is plotted as a function of time during the burst period. A 40% increase in area is observed during the burst. The growth of the L_β-phase domains can be explained by recent neutron diffraction results showing that a fraction of the hydrolysis products does not leave the membrane and accumulates at the L_β-phase interface (33).

However, the observation that the L_β phase grows during the hydrolytic burst and replaces the hydrolyzed fluid phase area is not consistent with the fact that a great fraction of the hydrolysis products, mostly lysolipids, should leave the membrane. If a bilayer configuration is maintained, the supported bilayer should not occupy the same surface area as the hydrolyzed membrane. Fig. 3 *c* shows a zoom out of the membrane 20 min after the end of the hydrolytic burst. The image shows the formation of large holes on the membrane. The height difference between the membrane surface and the bottom of the holes is ~40 Å, which corresponds to the typical thickness of the supported bilayer (20).

The percentage of area covered by the membrane after the hydrolytic burst was measured to be ~84.1 ± 0.9% and was found to be stable after the end of the hydrolytic burst. This implies that ~16% of the membrane surface area is lost during the hydrolytic burst. However, taking into account that only ~65% of the membrane surface area was in the L_β phase before adding the enzyme, it is clear that a large

fraction of the lipids that were originally in the fluid phase become adsorbed by the growing L_β-phase domains during the hydrolytic burst. These could be unhydrolyzed DMPC or DSPC molecules that migrate to the growing L_β domains. The growth of the L_β-phase domains could also be explained by the incorporation of fatty acids that are produced from the hydrolysis process. Although lysolipids that are produced by $sPLA_2$ tend to leave the membrane surface due to a high partitioning coefficient with water, fatty acids are more hydrophobic and exhibit a higher affinity for the membrane (33).

Hydrolysis of L_α domains by $sPLA_2$ in supported double bilayers that present $P_{\beta'}/L_\alpha$ phase coexistence

In Fig. 4, we monitor the hydrolysis of a $P_{\beta'}/L_\alpha$ domain structure at 30°C formed on the second bilayer in a supported double bilayer system. It has previously been shown that the behavior of a second supported bilayer resembles more closely the behavior of a free-standing bilayer (22). In particular, ripple formation is only observed in the second bilayer. In addition, the formation of anisotropic domains in DMPC/DSPC mixtures in giant unilamellar vesicles also only occurs in the second bilayer (20). We therefore expect the behavior of the second supported bilayer to reflect more closely the behavior of a free-standing bilayer during $sPLA_2$ hydrolysis.

It is important to avoid artifacts resulting from hydrolysis of the first supported bilayer as we study the evolution of the second bilayer. To do this, we have deposited a DSPC single bilayer by LB deposition before adding a second 1:1 DMPC/DSPC bilayer through vesicle fusion (see Materials and Methods). The DSPC bilayer is very resistant to hydrolysis at this temperature and will remain unaltered during $sPLA_2$ hydrolysis of the second bilayer.

Fig. 4 *a* (*upper left*) shows an AFM contact-mode image of the supported second bilayer at 32°C before addition of $sPLA_2$ and a deflection-mode image (*lower*), that is useful for discerning the presence of the ripple phase. The image shows the presence of ripple-phase domains in coexistence with the fluid-phase domains. There are two predominant ripple structures: the stable ripple phase (125 Å repeat distance between grooves) and the metastable ripple phase (250 Å repeat distance between grooves) (20,22). Depending on the thermal history of the sample, the two ripple phases can coexist. The image shows two distinct ordered phase regions—one elongated and one amorphous. A close-up of the deflection-mode image (data not shown) allows us to identify the elongated domain as containing the stable short-repeat-distance ripple structure, and the amorphous shaped regions as containing the metastable long-repeat-distance ripples. The formation of the elongated domain is induced by the stable phase ripples, which act as templates for domain growth (20).

After addition of $sPLA_2$, we observe a restructuring process (Fig. 4 *a*) that is qualitatively similar to the one observed in the single supported bilayer (Fig. 2). The L_α phase becomes preferentially hydrolyzed by $sPLA_2$, and the L_β phase (in this case the ripple phase) merges to reseal the membrane (see transition from −5 min to +8 min time points in Fig. 4 *a*). However, the images also show a restructuring of the ripple phase due to the hydrolytic activity of the enzyme (compare −5 min., +8 min, and +10 min (Fig. 4 *a*)) that occurs in parallel to the hydrolysis of the L_α phase (disappearance of the dark region observed at −5 min in Fig. 4 *a*). The ripple-phase spacing is observed to widen during $sPLA_2$ hydrolysis, and after a certain time point, the ripple-phase regions flatten and stabilize (+13 min in Fig. 4 *a*). The same restructuring process has been reported for a DMPC/DSPC membrane presenting only the ripple phase, in the absence of L_α-phase domains (22). The ripple restructuring process occurs in parallel with the preferential hydrolysis of the L_α phase. This indicates that the two distinct restructuring processes can occur independently in separate regions of the membrane.

Holes are observed to form on the membrane surface after the membrane stabilizes (+13 min in Fig. 4 *a*). It is reasonable for holes to form as the membrane hydrolysis products leave the surface. In Fig. 4 *c*, we indicate the position in the phase diagram where the images were taken, showing the fraction of fluid-phase domains predicted by the tie line. In Fig. 4 *d*, a comparison is made between 1), the fraction of fluid-phase lipids predicted by the tie line, 2), the fraction of fluid phase observed in the AFM images, and 3), the area fraction where holes are present after the hydrolytic burst. The hole fraction after the hydrolytic burst is similar to the area fraction occupied by the fluid phase before hydrolysis.

The lag time before the hydrolytic burst is drastically reduced in the double bilayer system (<3 min (Fig. 4 *b*)) compared to the single bilayer system (55–60 min (Figs. 2 *b* and 3 *b*) under the same reaction conditions). This indicates that the structural characteristics present in the second bilayer augment enzymatic activity. In particular, membrane packing levels are strong regulators of the hydrolytic activity (18). The presence of ripples, induced by the reduced interaction with the substrate in the second bilayer, may explain the presence of defects that augment enzyme activity. These results emphasize the advantages of the supported double bilayer system compared with the single-bilayer system when studying dynamic restructuring of a membrane. The double-bilayer system will reflect more closely the behavior of free-standing membranes.

Preferential hydrolysis of the L_α phase in the presence of lipid domains leads to an increase in membrane order

In Figs. 5 and 6, we relate the findings obtained by AFM to lipid suspensions treated with $sPLA_2$. We utilize 200-nm LUVs to ensure the formation of the ripple phase (22). The AFM results indicate that the enzyme, in the presence

of L_α/L_β coexisting domains, should preferentially hydrolyze the L_α phase. Earlier reports analyzing sPLA$_2$ hydrolysis in mixed monolayers have shown that subtle differences in lipid packing induce preferential hydrolysis of one of the lipid components (34) Therefore, it would be expected that domain formation would result in the preferential hydrolysis of the lipid component that is enriched in the liquid-disordered phase; in this case DMPC. In Fig. 5, we measure DMPC (Fig. 5 *a*) and DSPC (Fig. 5 *b*) hydrolysis levels after the sPLA$_2$ burst for different compositional points in the DMPC/DSPC phase diagram.

The burst is determined by fluorescence spectroscopy, and the enzymatic reaction is quenched by addition of EDTA at well-defined time points after the burst. The circles represent the percentage of lipid hydrolyzed at a particular compositional point. It is clear from a comparison of Fig. 5, *a* and *b*, that although the level of hydrolysis of DMPC does not vary significantly throughout the L_α/L_β phase coexistence regime, DSPC shows a sharp reduction in the level of hydrolysis for tie lines close to the solidus phase line. These results fit well with the AFM results, since at these temperatures, the tie lines indicate that the L_α-phase domains that are being hydrolyzed are enriched in DMPC. For example, at 30°C, the L_α-phase domains contain ~90% DMPC, as determined from the intersection of the tie line with the fluidus-phase boundary in Fig. 5 *a*. A very small percentage of DSPC will be susceptible to hydrolysis for these compositions. It is unclear why close to the fluidus-phase line there is an increase in the percentage of DSPC hydrolyzed even though, as is evident from the phase diagram, the coexisting domains maintain the composition specified by the tie line at a given temperature (see horizontal progression of the level of hydrolysis at 45°C in Fig. 5 *b*). This may be due to the fluctuating character of the domain structure close to the fluidus-phase boundary line, which may result in DSPC becoming transiently susceptible to hydrolysis (10).

The L_α- and L_β-phase regions outside the coexistence regime show either low levels of hydrolysis for both lipids or no hydrolytic activity (Fig. 5, *crosses*). This is expected, since one-phase regions present a homogeneous lipid arrangement, and the lag time becomes very long. It is well known that the lack of defects in membrane composition causes reduced enzymatic activity (18). On the other hand, the domain interface regions in the two-phase coexistence regimes provide defects that increase the hydrolysis rate. Previously, we reported that within the ripple-phase region, a high level of hydrolysis is observed for DMPC compared to DSPC. This is also evident from the data point at 50:50 DMPC/DSPC at 25°C in Fig. 5 (22). This result may be due to the structural nature of the ripple phase (25), which could result in preferred hydrolysis of fluidlike regions within the ripple structure. However, further experiments exploring hydrolysis of the components in the mixture in relation to the phase diagram are needed to explore this hypothesis.

The fact that sPLA$_2$ preferentially hydrolyzes DMPC implies that during the enzymatic process, the membrane will become enriched in the higher melting component. We propose that this would lead to an increase in membrane

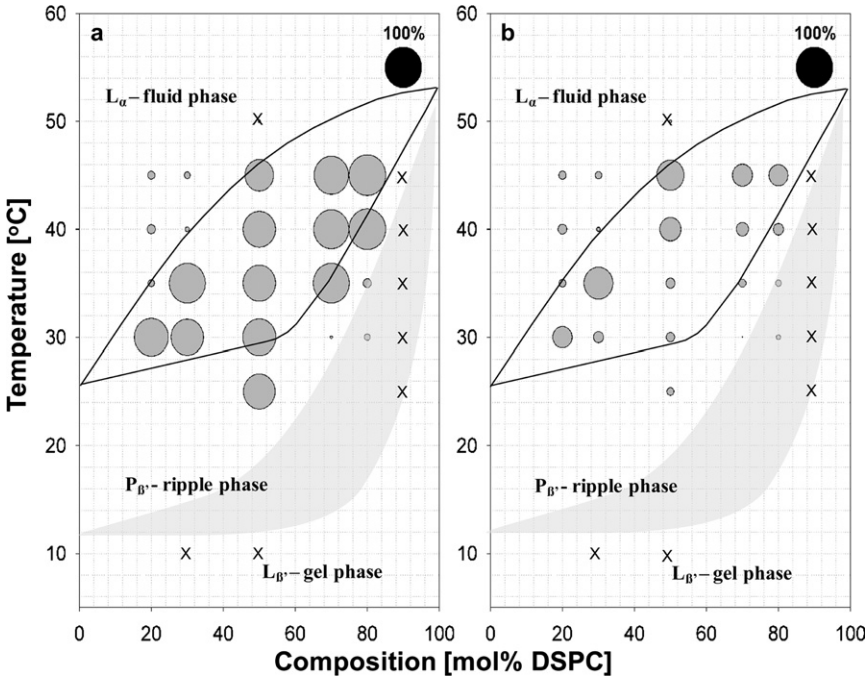

FIGURE 5 Map of hydrolysis levels for (*a*) DMPC and (*b*) DSPC at different compositions and temperatures encompassing the L_α/L_β coexistence regime in the DMPC/DSPC phase diagram. The size of the circles on the phase diagram indicates the level of hydrolysis for each component at that particular composition and temperature, with the black circle at upper right representing 100% hydrolysis. Crosses indicate points in the phase diagram where no hydrolytic activity was detected.

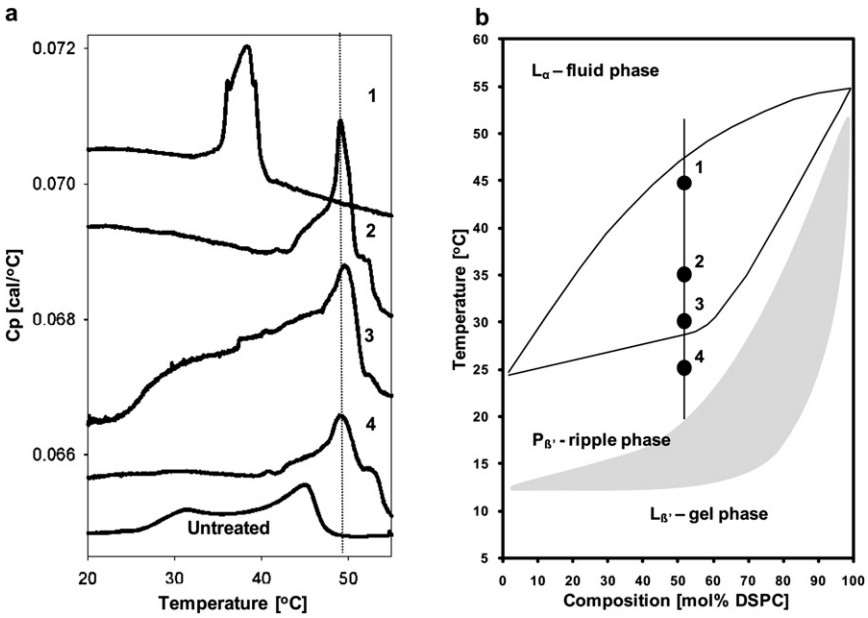

FIGURE 6 (*a*) Differential scanning calorimetry thermograms are shown for 1:1 DMPC/DSPC unilamellar vesicles before treatment with $sPLA_2$ (*Untreated*) and after treatment with $sPLA_2$ (1–4) at different temperature points as indicated in the DMPC/DSPC phase diagram in *b*.

rigidity indicated by an increase in the melting temperature of the mixture. We explore this process by measuring DSC thermograms of samples after treatment with $sPLA_2$ at different temperatures (Fig. 6). The phase diagram in Fig. 6 *b* indicates the composition and treatment temperature of four different samples of unilamellar vesicles. The DSC trace for unilamellar vesicles before $sPLA_2$ treatment is shown at the bottom of Fig. 6 *a* (*Untreated*). This is a DSC trace of the unilamellar vesicle suspension, and for this reason, the melting events are not as cooperative as those observed for multilamellar vesicles (10). However, the pretransition and L_α/L_β coexistence regime are still clearly distinguished. After the hydrolytic burst of $sPLA_2$, we observe clear differences in the end-product DSC traces for the different samples depending on the original position in the phase diagram. After hydrolysis of sample 1 (treated with $sPLA_2$ at 45°C), we find the emergence of a broad peak in the specific heat capacity at constant pressure near 37°C. This peak is centered in the coexistence region of the original sample (*Untreated*). As shown in Fig. 5, at 45°C, $sPLA_2$ hydrolyzes both lipids equally, as indicated by the similar size of the circles. Samples 2–4 (treated at 25°C, 30°C, and 35°C, respectively) show a shift toward the higher melting transition corresponding to DSPC. These results indicate that $sPLA_2$ hydrolysis in the presence of lipid domains close to the solidus line (samples 2 and 3) generates an increase in the melting-transition temperature of the sample due to enrichment in the higher melting lipid. Sample 4, which starts out in the ripple phase regime, also shows an increase in melting temperature, which is consistent with our previous result showing preferential hydrolysis of DMPC in the ripple regime (22). The results of Fig. 6 indicate that $sPLA_2$ can act as a membrane-rigidifying agent in the case where lipid domains are present and the enzyme hydrolyzes the more fluid lipid phase.

CONCLUSION

In this work, we investigate enzyme-induced dynamic restructuring in the presence of L_α/L_β-phase domains. We observed that the enzyme preferentially hydrolyzes the L_α-phase regions, and that during the hydrolysis of these regions the membrane is capable of resealing. The enzymatic activity induces a compositional transition from a membrane presenting L_α/L_β domain coexistence to a membrane fully in the L_β phase through an enrichment in the higher-melting-temperature component while maintaining membrane integrity. This enrichment in the higher-melting-temperature component is not observed in the absence of lipid domains. Domain formation can therefore be used to direct the end-product of the hydrolytic process by generating preferential hydrolysis of specific components in the membrane.

The results also show that supported lipid bilayers formed by vesicle fusion instead of LB deposition provide a dynamic membrane system adapted for investigating membrane-restructuring processes by AFM. As shown in previous publications, $sPLA_2$ hydrolysis of LB membranes results in the formation of holes, which are not capable of resealing dynamically (29). In contrast, membranes formed by vesicle fusion reseal in a fashion similar to that of free-standing membranes during the hydrolytic process. The second supported bilayer in a double-bilayer system shows even faster dynamics than a single supported bilayer, indicating that the reduced interactions resulting from the increased separation of the bilayer from the support provides a more dynamic system.

Previous studies have reported on the regulation of $sPLA_2$ activity through the presence of lipid domains. However, these studies focus mainly on the conditions necessary for triggering or inhibiting enzyme activity. In this report, we focus on how the enzymatic activity, once triggered, can be directed to generate a specific end-product. Domain formation can therefore act as a mechanism for generating an enrichment of certain lipid components during the hydrolytic process, which in this case generates an increase in membrane rigidity through an enrichment in the higher-melting-temperature component.

This research was supported by a grant from COLCIENCIAS. We acknowledge support from the Danish National Research foundation via a grant to MEMPHYS-Center for Biomembrane Physics.

REFERENCES

1. Schaloske, R. H., and E. A. Dennis. 2006. The phospholipase A2 superfamily and its group numbering system. *Biochim. Biophys. Acta.* 1761:1246–1259.
2. Brueseke, T. J., and J. D. Bell. 2006. A new hat for an old enzyme: waste management. *Biochim. Biophys. Acta.* 1761:1270–1279.
3. Geddis, M. S., and V. Rehder. 2003. Initial stages of neural regeneration in *Helisoma trivolvis* are dependent upon PLA2 activity. *J. Neurobiol.* 54:555–565.
4. Nevalainen, T. J., M. M. Haapamäki, and J. M. Grönroos. 2000. Roles of secretory phospholipases A(2) in inflammatory diseases and trauma. *Biochim. Biophys. Acta.* 1488:83–90.
5. Buckland, A. G., E. L. Heeley, and D. C. Wilton. 2000. Bacterial cell membrane hydrolysis by secreted phospholipases A(2): a major physiological role of human group IIa sPLA(2) involving both bacterial cell wall penetration and interfacial catalysis. *Biochim. Biophys. Acta.* 1484:195–206.
6. van den Brink-van der Laan, E., J. A. Killian, and B. de Kruijff. 2004. Nonbilayer lipids affect peripheral and integral membrane proteins via changes in the lateral pressure profile. *Biochim. Biophys. Acta.* 1666:275–288.
7. Epand, R. M., N. Fuller, and R. P. Rand. 1996. Role of the position of unsaturation on the phase behavior and intrinsic curvature of phosphatidylethanolamines. *Biophys. J.* 71:1806–1810.
8. Kooijman, E. E., V. Chupin, …, P. R. Rand. 2005. Spontaneous curvature of phosphatidic acid and lysophosphatidic acid. *Biochemistry.* 44:2097–2102.
9. Henriksen, J., A. C. Rowat, and J. H. Ipsen. 2004. Vesicle fluctuation analysis of the effects of sterols on membrane bending rigidity. *Eur. Biophys. J.* 33:732–741.
10. Leidy, C., W. F. Wolkers, …, J. H. Crowe. 2001. Lateral organization and domain formation in a two-component lipid membrane system. *Biophys. J.* 80:1819–1828.
11. Bagatolli, L. A., and E. Gratton. 2000. Two photon fluorescence microscopy of coexisting lipid domains in giant unilamellar vesicles of binary phospholipid mixtures. *Biophys. J.* 78:290–305.
12. de Almeida, R. F. M., A. Fedorov, and M. Prieto. 2003. Sphingomyelin/phosphatidylcholine/cholesterol phase diagram: boundaries and composition of lipid rafts. *Biophys. J.* 85:2406–2416.
13. Wei, S., W. Y. Ong, …, W. Hong. 2003. Group IIA secretory phospholipase A2 stimulates exocytosis and neurotransmitter release in pheochromocytoma-12 cells and cultured rat hippocampal neurons. *Neuroscience.* 121:891–898.
14. Hønger, T., K. Jørgensen, …, O. G. Mouritsen. 1996. Systematic relationship between phospholipase A2 activity and dynamic lipid bilayer microheterogeneity. *Biochemistry.* 35:9003–9006.
15. Burack, W. R., Q. Yuan, and R. L. Biltonen. 1993. Role of lateral phase separation in the modulation of phospholipase A2 activity. *Biochemistry.* 32:583–589.
16. Burack, W. R., and R. L. Biltonen. 1994. Lipid bilayer heterogeneities and modulation of phospholipase A2 activity. *Chem. Phys. Lipids.* 73:209–222.
17. Bell, J. D., M. Burnside, …, M. L. Baker. 1996. Relationships between bilayer structure and phospholipase A2 activity: interactions among temperature, diacylglycerol, lysolecithin, palmitic acid, and dipalmitoylphosphatidylcholine. *Biochemistry.* 35:4945–4955.
18. Jensen, L. B., N. K. Burgess, …, J. D. Bell. 2005. Mechanisms governing the level of susceptibility of erythrocyte membranes to secretory phospholipase A2. *Biophys. J.* 88:2692–2705.
19. Simonsen, A. C. 2008. Activation of phospholipase A2 by ternary model membranes. *Biophys. J.* 94:3966–3975.
20. Leidy, C., T. Kaasgaard, …, K. Jørgensen. 2002. Ripples and the formation of anisotropic lipid domains: imaging two-component supported double bilayers by atomic force microscopy. *Biophys. J.* 83:2625–2633.
21. Kaasgaard, T., C. Leidy, …, K. Jørgensen. 2003. Temperature-controlled structure and kinetics of ripple phases in one- and two-component supported lipid bilayers. *Biophys. J.* 85:350–360.
22. Leidy, C., O. G. Mouritsen, …, G. H. Peters. 2004. Evolution of a rippled membrane during phospholipase A2 hydrolysis studied by time-resolved AFM. *Biophys. J.* 87:408–418.
23. Høyrup, P., J. Davidsen, and K. Jørgensen. 2001. Lipid membrane partitioning of lysolipids and fatty acids: effects of membrane phase structure and detergent chain length. *J. Phys. Chem. B.* 105:2649–2657.
24. Mabrey, S., and J. M. Sturtevant. 1976. Investigation of phase transitions of lipids and lipid mixtures by sensitivity differential scanning calorimetry. *Proc. Natl. Acad. Sci. USA.* 73:3862–3866.
25. Heimburg, T. 2000. A model for the lipid pretransition: coupling of ripple formation with the chain-melting transition. *Biophys. J.* 78:1154–1165.
26. Knoll, W., K. Ibel, and E. Sackmann. 1981. Small-angle neutron scattering study of lipid phase diagrams by the contrast variation method. *Biochemistry.* 20:6379–6383.
27. Ratto, T. V., and M. L. Longo. 2002. Obstructed diffusion in phase-separated supported lipid bilayers: a combined atomic force microscopy and fluorescence recovery after photobleaching approach. *Biophys. J.* 83:3380–3392.
28. Giocondi, M. C., and C. Le Grimellec. 2004. Temperature dependence of the surface topography in dimyristoylphosphatidylcholine/distearoylphosphatidylcholine multibilayers. *Biophys. J.* 86:2218–2230.
29. Nielsen, L. K., J. Risbo, …, T. Bjørnholm. 1999. Lag-burst kinetics in phospholipase A(2) hydrolysis of DPPC bilayers visualized by atomic force microscopy. *Biochim. Biophys. Acta.* 1420:266–271.
30. Hønger, T., K. Jørgensen, …, O. G. Mouritsen. 1997. Phospholipase A2 activity and physical properties of lipid-bilayer substrates. *Methods Enzymol.* 286:168–190.
31. Sanchez, S. A., L. A. Bagatolli, …, T. L. Hazlett. 2002. A two-photon view of an enzyme at work: *Crotalus atrox* venom PLA2 interaction with single-lipid and mixed-lipid giant unilamellar vesicles. *Biophys. J.* 82:2232–2243.
32. Kaasgaard, T., J. H. Ipsen, …, K. Jørgensen. 2001. In situ atomic force microscope imaging of phospholipase A2 hydrolysis of one and two-component lipid bilayers. *J. Probe Microsc.* 2:169–175.
33. Wacklin, H. P., F. Tiberg, …, R. K. Thomas. 2007. Distribution of reaction products in phospholipase A2 hydrolysis. *Biochim. Biophys. Acta.* 1768:1036–1049.
34. Grainger, D. W., A. Reichert, …, J. B. Lloyd. 1990. Mixed monolayers of natural and polymeric phospholipids: structural characterization by physical and enzymatic methods. *Biochim. Biophys. Acta.* 1022:146–154.